THE JOURNAL OF BIOLOGICAL CHEMISTRY VOL. 286, NO. 13, pp. 11792–11802, April 1, 2011

Modulatory ATP Binding Affinity in Intermediate States of *E*2P Dephosphorylation of Sarcoplasmic Reticulum Ca^{2+}-ATPase*[S]

Received for publication, November 23, 2010, and in revised form, January 20, 2011 Published, JBC Papers in Press, February 2, 2011, DOI 10.1074/jbc.M110.206094

Johannes D. Clausen[‡1], **David B. McIntosh**[§], **David G. Woolley**[§], **and Jens Peter Andersen**[‡2]

From the [‡]*Department of Physiology and Biophysics, Aarhus University, DK-8000 Aarhus C, Denmark and the* [§]*Institute of Infectious Diseases and Molecular Medicine, Division of Chemical Pathology, Faculty of Health Sciences, University of Cape Town, Observatory, Cape Town 7925, South Africa*

The mechanism of ATP modulation of *E*2P dephosphorylation of sarcoplasmic reticulum Ca^{2+}-ATPase wild type and mutant forms was examined in nucleotide binding studies of states analogous to the various intermediates of the dephosphorylation reaction, obtained by binding of metal fluorides, vanadate, or thapsigargin. Wild type Ca^{2+}-ATPase displays an ATP affinity of 4 μM for the *E*2P ground state analog, 1 μM for the *E*2P transition state and product state analogs, and 11 μM for the *E*2 dephosphoenzyme. Hence, ATP binding stabilizes the transition and product states relative to the ground state, thereby explaining the accelerating effect of ATP on dephosphorylation. Replacement of Phe^{487} (N-domain) with serine, Arg^{560} (N-domain) with leucine, or Arg^{174} (A-domain) with alanine or glutamate reduces ATP affinity in all *E*2/*E*2P intermediate states. Alanine substitution of Ile^{188} (A-domain) increases the ATP affinity, although ATP acceleration of dephosphorylation is disrupted, thus indicating that the critical role of Ile^{188} in ATP modulation is mechanistically based rather than being associated with the binding of nucleotide. Mutants with alanine replacement of Lys^{205} (A-domain) or Glu^{439} (N-domain) exhibit an anomalous inhibition by ATP of *E*2P dephosphorylation, due to ATP binding increasing the stability of the *E*2P ground state relative to the transition state. The ATP affinity of Ca_2*E*2P, stabilized by inserting four glycines in the A-M1 linker, is similar to that of the *E*2P ground state, but the Ca^{2+}-free *E*1 state of this mutant exhibits 3 orders of magnitude reduction of ATP affinity.

The sarco(endo)plasmic reticulum Ca^{2+}-ATPase (Ca^{2+}-ATPase)[3] is a membrane-bound P-type ATPase that translocates Ca^{2+} from the cytosol to the endoplasmic reticulum, thereby allowing rapid oscillations of Ca^{2+} during cellular activation events. Insight into the structural organization of the Ca^{2+}-ATPase has come from the elucidation of several crystal structures at atomic resolution, representing the pump in various intermediate states (reviewed in Refs. 1 and 2). The membrane-buried region of the Ca^{2+}-ATPase is made up of 10 membrane spanning helices and is connected to a large cytoplasmic headpiece, which is further separated into three distinct domains, denoted A ("actuator"), P ("phosphorylation"), and N ("nucleotide binding"). Ca^{2+} transport is achieved by means of a reaction cycle (Scheme 1) involving the formation and decay of a phosphorylated intermediate and extensive protein conformational changes between four major states, *E*1, *E*1P, *E*2P, and *E*2. The catalytic function in *E*1 (autokinase activity) and *E*2P (autophosphatase activity) as well as the movement of Ca^{2+} ions across the membrane can be understood on the basis of the sequential gathering and displacement of certain conserved amino acid motifs of the N- and A-domains relative to the catalytic site in the P-domain and the coupling of these events to rearrangements of the transmembrane helices containing the Ca^{2+} sites. In the *E*1 and *E*1P states, the highly conserved ^{181}TGES loop of the A-domain is distant from the catalytic center containing nucleotide binding residues and the phosphorylated Asp^{351} of the P-domain, which in this condition is able to react with ATP/ADP. However, during the Ca_2*E*1P → *E*2P transition the A domain rotates ~90° around an axis nearly perpendicular to the membrane, thereby moving the ^{181}TGES loop into close contact with the catalytic site, such that Glu^{183} can catalyze dephosphorylation of *E*2P by hydrolysis (3–5). During the dephosphorylation, Glu^{183} likely coordinates the water molecule attacking the aspartyl phosphoryl bond and withdraws a hydrogen.

ATP in addition to being the substrate in the phosphorylation of the Ca_2*E*1 state also functions in a non-phosphorylating mode (*boxed ATP* in Scheme 1), enhancing the rates of the steps involved in phosphoenzyme turnover (Ca_2*E*1P → *E*2P and *E*2P → *E*2) as well as the *E*2 → Ca_2*E*1 transition of the dephosphoenzyme (6–17). The mechanisms underlying these modulatory effects of ATP remain largely unresolved. A debated issue is whether the modulatory ATP molecule binds at the same site as the phosphorylating ATP or at a distinct, "allosteric" site (14, 18–23). During dephosphorylation the ^{181}TGES loop of the A-domain occupies the position in close contact with the P-domain taken up by part of the ATP and ADP in Ca_2*E*1 and Ca_2*E*1P, however, ATP may still bind to residues of the N- and

* This work was supported in part by grants from the Danish Medical Research Council (to J. P. A.), the Novo Nordisk Foundation (to J. P. A.), and the Danish National Research Foundation (PUMPKIN Centre).

[S] The on-line version of this article (available at http://www.jbc.org) contains supplemental Table S1 and Figs. S1–S8.

[1] Supported by the Centre for Membrane Pumps in Cells and Disease, PUMPKIN, Danish National Research Foundation.

[2] To whom correspondence should be addressed: Ole Worms Allé 6, Bldg. 1180, DK-8000 Aarhus C, Denmark. Fax: 45-86129065; E-mail: jpa@fi.au.dk.

[3] The abbreviations used are: Ca^{2+}-ATPase, Ca^{2+}-transporting adenosine triphosphatase (EC 3.6.3.8); AlF, complex of Al^{3+} and fluoride; AMPPCP, adenosine 5′-(β,γ-methylene)triphosphate; BeF, complex of Be^{2+} and fluoride; EPPS, *N*-2-hydroxyethylpiperazine-*N*′-3-propanesulfonic acid; MgF, complex of Mg^{2+} and fluoride; MOPS, 3-(*N*-morpholino)propanesulfonic acid; SR, sarcoplasmic reticulum vesicles purified from rabbit hind leg muscle; Tg, thapsigargin; TNP-8N_3-ATP, 2′,3′-*O*-(2,4,6-trinitrophenyl)-8-azidoadenosine 5′-triphosphate; WT, wild type Ca^{2+}-ATPase.

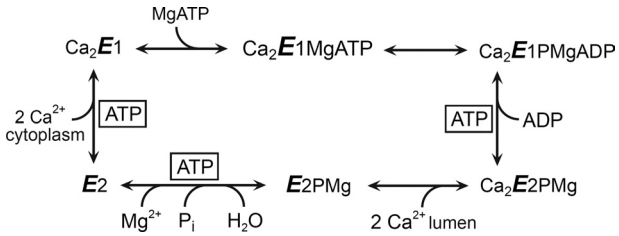

SCHEME 1. **Ca^{2+}-ATPase reaction cycle.** Major conformational changes and substrate binding and dissociation steps are shown. *Boxed ATP* indicates steps for which the rate is enhanced by additional binding of ATP or MgATP that is not hydrolyzed ("modulatory ATP").

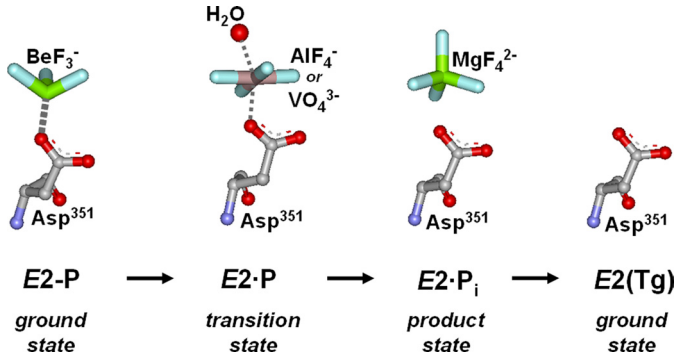

SCHEME 2. **Molecular details of the *E*2P dephosphorylation reaction sequence.** Stable analogs of intermediate states of the *E*2P → *E*2 reaction sequence can be formed by incubation of the Ca^{2+}-ATPase with BeF (*E*2P ground state), AlF (*E*2·P transition state), vanadate (*E*2·P transition state), MgF (*E*2·P_i product state), and Tg (*E*2 ground state) in the absence of Ca^{2+} (25, 28).

A-domains under these conditions. Recently, mutagenesis studies have pinpointed several amino acid residues in the N- and A-domains as critical for the modulatory effects of ATP and have provided evidence of an overlap between the catalytic and modulatory ATP binding sites (16, 17, 24), *i.e.* favoring the existence of a single site that exhibits a high degree of plasticity and flexibility, being reconfigured from slightly different positions of the P-, N-, and A-domains in the conformational states occurring during the transport cycle. The conformational transitions of the cycle likely change the affinity of the site for ATP, thus explaining the enhancing effects of ATP on the kinetics. Hence, the forward flow of a reversible reaction will be enhanced by ATP, if the product state possesses higher affinity for ATP than the ground state (23). Moreover, a relative stabilization of the transition state of a partial reaction of the cycle, leading to acceleration of this reaction, would be achieved in the presence of ATP, if ATP bound with higher affinity to the transition state than to the corresponding ground state. In the present study we have focused on the role of ATP as a modulator of *E*2P dephosphorylation. We present, for the first time, direct measurements of the ATP affinity of wild type and mutant Ca^{2+}-ATPases stabilized in states analogous to the various intermediate forms occurring during the *E*2P dephosphorylation reaction sequence. This was achieved by use of the metal-fluoride compounds BeF, AlF, and MgF (Scheme 2) to mimic the phosphoryl group in the ground, transition, and product states of *E*2P dephosphorylation, respectively (4, 5, 25, 26), and vanadate, which like AlF is thought to mimic the bipyramidal transition state of the phosphoryl group (27, 28). The ATP affinity was also determined for a stable form of the *E*2 dephosphoenzyme obtained by binding of thapsigargin (29, 30) and for the Ca_2*E*2P phosphoenzyme intermediate that still has Ca^{2+} bound. The latter was stabilized by inserting four glycines in the A-M1 linker (mutation "4Gi-46/47") (31, 32). For these stable states the affinity constants for ATP could be determined by studying the competitive inhibition by ATP of TNP-8N_3-ATP photolabeling of Lys^{492}, an assay that has proven very powerful for determination of nucleotide affinity of the *E*1 state of expressed wild type and mutant Ca^{2+}-ATPases (*e.g.* Refs. 33 and 34), but has not previously been applied to the phosphoenzyme or analog states of intermediates of *E*2P dephosphorylation. We demonstrate that, for the wild type Ca^{2+}-ATPase, the affinity for modulatory ATP varies during the dephosphorylation sequence, being intermediate in the *E*2P ground state (with or without bound Ca^{2+}), highest in the *E*2P transition and product states, and lowest in the *E*2 dephosphoenzyme. Our analysis of mutant Ca^{2+}-ATPases provides insight into the varying contributions by individual amino acid residues to nucleotide binding during the dephosphorylation reaction sequence and allows distinction between roles in nucleotide binding and in mediating the response to binding that accelerates the dephosphorylation.

EXPERIMENTAL PROCEDURES

The cDNA encoding the mutant Ca^{2+}-ATPases studied in the present work was the same as that applied in our previous studies (16, 17, 33–35). The cDNA was inserted into the expression vector pMT2 (36). To express wild type and mutant cDNA, COS-1 cells were transfected using the calcium phosphate precipitation method (37). Microsomal vesicles containing either expressed wild type or mutant Ca^{2+}-ATPase were isolated by differential centrifugation (38). SR vesicles isolated from rabbit hind leg muscles (prepared as described in Refs. 39 and 40)) were a gift from Dr. Philippe Champeil (Saclay, France). The concentration of expressed Ca^{2+}-ATPase was determined by an enzyme-linked immunosorbent assay (41) and by measurement of the maximum capacity for phosphorylation with ATP or P_i ("active site concentration" (42)). As previously described, the expression levels of the mutants were similar to that of the wild type (16, 17, 33, 34). The amount of endogenous endoplasmic reticulum Ca^{2+}-ATPase present in the preparation is less than 1% that of the exogenous expressed enzyme, hence labeling corresponding to endogenous Ca^{2+}-ATPase is negligible (*cf.* Fig. 1 of Ref. 33, compare "wild type" with "control").

Formation of the complexes of SR or expressed wild type or mutant Ca^{2+}-ATPase in the *E*2 state with Tg, MgF, AlF, vanadate, and BeF prior to photolabeling was achieved by pre-equilibration of the enzyme for 30 min at 25 °C in 25 mM MOPS/tetramethyl ammonium hydroxide (pH 7.0), 80 mM KCl, 2 mM EGTA, and the concentrations of inhibitors and co-factors indicated as follows: Tg, 1 μM Tg; MgF, 5 mM $MgCl_2$ and 5 mM NaF; vanadate, 0.1 mM orthovanadate and 5 mM $MgCl_2$; AlF, 0.5 mM $AlCl_3$, 2 mM NaF, and 0.2 mM $MgCl_2$; BeF, 0.1 mM $BeSO_4$, 2 mM NaF, and 0.2 mM $MgCl_2$. The enzyme-inhibitor complexes were formed immediately prior to the initiation of the photolabeling experiments and kept on ice throughout (<1 h). The inhibited state of wild type and mutants at the inhibitor concentrations applied, as well as the stability of the enzyme-inhib-

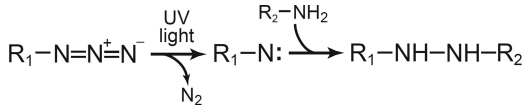

SCHEME 3. **TNP-8N_3-ATP photolabeling reaction.** When the azide of TNP-8N_3-ATP is exposed to ultraviolet light, it forms a highly reactive but short-lived nitrene that can initiate reactions with neighboring reactive groups, such as the amino group of the Lys^{492} side chain, thereby forming a stable covalent bond between the nucleotide and the protein (20, 45, 46). R_1 represents the TNP-ATP moiety of TNP-8N_3-ATP (see supplemental Fig. S4), and R_2-NH_2 is the Lys^{492} side chain of the Ca^{2+}-ATPase.

itor complexes under photolabeling conditions, is validated under supplemental Table S1 and Figs. S1 and S2).

The synthesis of the [γ-^{32}P]TNP-8N_3-ATP photolabel, its application as a specific photolabel of the Ca^{2+}-ATPase (Scheme 3), the competitive inhibition by ATP of [γ-^{32}P]TNP-8N_3-ATP photolabeling, and the quantification of ^{32}P-labeled bands by electronic autoradiography following SDS-PAGE were carried out using the previously established procedures (20, 33). The medium used for photolabeling contained 25 mM EPPS/tetramethyl ammonium hydroxide (pH 8.5), 2 mM EDTA (to remove Ca^{2+} and any Mg^{2+} not tightly bound in the enzyme-inhibitor complex), 17.4% (v/v) glycerol, and [γ-^{32}P]TNP-8N_3-ATP without or with ATP at the concentrations indicated in the figures. For photolabeling in the presence of Mg^{2+}, 2 mM EDTA was replaced by 1 mM $MgCl_2$ and 0.5 mM EGTA. The concentration of [γ-^{32}P]TNP-8N_3-ATP used in competition experiments with ATP was 3× the $K_{0.5}$, where $K_{0.5}$ is the [γ-^{32}P]TNP-8N_3-ATP concentration giving half-maximum labeling. For photolabeling the enzyme was diluted 25-fold into ice-cold labeling medium immediately prior to irradiation. The concentration of Ca^{2+}-ATPase in the final photolabeling mixture was typically ~2 nM. Such low Ca^{2+}-ATPase concentration was critical, because of the high TNP-8N_3-ATP affinity of certain mutants (in some cases, $K_{0.5}$ values as low as 5 nM were obtained, as demonstrated below). Irradiations were performed in a total volume of 75 μl in an ice-cold 500-μl quartz cuvette using the collimated light beam from an LSH102 Arc Light Source (LOT-Oriel Group Europe, Darmstadt, Germany) assembled with a 150 W ozone-free xenon arc lamp, a rear light reflector, an F/1.3 35-mm aperture quartz condenser, and a glass filter with 295-nm wavelength cut-off. The power supply was adjusted to 38 W and the irradiation time was 35 s, unless stated otherwise. The cuvette was placed at a fixed position 5 cm from the tip of the filter holder mounted in front of the condenser. The diameter of the collimated light beam covered the entire reaction volume contained in the cuvette. The irradiation setup was kept fixed for all photolabeling experiments carried out in the present study. The experiment shown in supplemental Fig. S3 confirms that the 35-s irradiation time generally used in the photolabeling experiments did not affect the activity of the enzyme substantially.

To form the Ca_2E2P state of mutant 4Gi-46/47 (31, 35), phosphorylation was carried out for 10 min at 25 °C in 25 mM MOPS/tetramethyl ammonium hydroxide (pH 7.0), 10 mM $MgCl_2$, 15% DMSO, 38 μM calcium ionophore A23187, 1 mM EGTA, and 0.5 mM P_i, followed by cooling on ice. Immediately prior to photolabeling, 2 μl of the phosphorylated microsomes were supplemented with 2 μl of ice-cold 42 mM $CaCl_2$, to give a final free Ca^{2+} concentration of 20.5 mM (on both the lumenal and the cytoplasmic sides of the membrane, because of the presence of the calcium ionophore). Then, 3 μl of the phosphorylated and Ca^{2+}-saturated enzyme were diluted 25-fold into the premixed photolabeling medium, followed by irradiation.

Measurements of phosphorylation from [γ-^{32}P]ATP or $^{32}P_i$ were carried out by acid quenching followed by acid SDS-polyacrylamide gel electrophoresis and quantification of the radioactivity associated with the Ca^{2+}-ATPase band, using the previously established procedures (16, 17, 43). To study the ATP concentration dependence of phosphorylation, microsomes were incubated for 15 s at 0 °C in 40 mM MOPS/Tris (pH 7.0), 80 mM KCl, 5 mM $MgCl_2$, 100 μM $CaCl_2$, and varying concentrations of [γ-^{32}P]ATP. For studies of the ATP dependence of dephosphorylation of *E*2P, phosphorylation with 0.5 mM $^{32}P_i$ was carried out for 10 min at 25 °C in 100 mM MES/Tris (pH 6.0), 10 mM $MgCl_2$, 2 mM EGTA, and 30% (v/v) dimethyl sulfoxide. The phosphorylated sample was chilled in ice water, and dephosphorylation was followed at 0 °C by a 19-fold dilution into ice-cold medium containing 50 mM MOPS/Tris (pH 7.0), 2 mM EGTA, 10 mM EDTA, 5 mM H_3PO_4, and various concentrations of ATP.

The data were analyzed by nonlinear regression using the SigmaPlot program (SPSS, Inc.). The analysis of the TNP-8N_3-ATP photolabeling data were based on the hyperbolic function, $Y = Y_{max} \times [\text{TNP-8}N_3\text{-ATP}]/(K_{0.5} + [\text{TNP-8}N_3\text{-ATP}]) + m \times [\text{TNP-8}N_3\text{-ATP}]$, in which Y is the amount of photolabeled Ca^{2+}-ATPase, Y_{max} is the maximum amount of photolabeled Ca^{2+}-ATPase, $K_{0.5}$ is the concentration of TNP-8N_3-ATP giving half-maximum labeling, and $m \times$ [TNP-8N_3-ATP] is a linear component, which has been subtracted from the data shown (33). The analysis of the data obtained from ATP inhibition of TNP-8N_3-ATP photolabeling was based on the Hill equation modified to describe inhibition, $Y = Y_{max} \times (1 - [\text{ATP}]^n/(K_{0.5}{}^n + [\text{ATP}]^n))$, in which Y and Y_{max} are defined as above, $K_{0.5}$ is the concentration of ATP giving half-maximum effect, and n is the Hill coefficient (varying between 0.6 and 1.1 for the present data). The "true" dissociation constant, K_D, for ATP binding was calculated from the measured $K_{0.5}$ values using the validated equation for competitive inhibition (33). The analysis of the ATP dependence of phosphorylation from [γ-^{32}P]ATP was based on the Hill equation, $EP = EP_{max} \times [\text{ATP}]^n/(K_{0.5}{}^n + [\text{ATP}]^n)$. For analysis of the modulatory effect of ATP on the rate of *E*2P dephosphorylation, the ATP concentration dependence of the rate constant was analyzed according to the hyperbolic function, $k_{obs} = k_0 + (k_{max} - k_0) \times [\text{ATP}]/(K_{0.5} + [\text{ATP}])$, in which k_{obs} is the rate constant observed at the indicated ATP concentration, k_0 is the rate constant in the absence of ATP, and k_{max} is the extrapolated value of the rate constant corresponding to infinite ATP concentration (17). The experiments were conducted at least twice on independent microsomal preparations, and average values are shown.

RESULTS AND DISCUSSION

TNP-8N_3-ATP Photolabeling of Wild Type Ca^{2+}-ATPase in E2·Tg, E2·MgF, E2·Vanadate, E2·AlF, and E2·BeF States—To study the interaction of nucleotides with the wild type Ca^{2+}-ATPase in stable analog forms of the intermediate states occur-

ring during *E*2P dephosphorylation, SR vesicles or microsomes containing expressed enzyme were incubated with saturating concentrations of Tg, MgF, vanadate, AlF, or BeF and subjected to nucleotide binding analysis by TNP-$8N_3$-ATP photolabeling of Lys^{492} as previously described for the *E*1 form (33). The formation of the complex with metal fluoride or vanadate took place in the presence of Mg^{2+}, whereas subsequent photolabeling was carried out in medium without free Mg^{2+} (EDTA added), considering that the substrate that binds to *E*2P with reasonable affinity and accelerates *E*2P dephosphorylation is metal-free ATP (10, 14, 15). Enzyme with Tg bound and enzyme in the *E*1 form was photolabeled either in the absence or presence of Mg^{2+}. In the latter case, EGTA was present to specifically chelate Ca^{2+}, because it was essential to remove Ca^{2+} to prevent enzyme activation and consequent hydrolysis of the photolabel and ATP. Photolabeling was carried out at a rather high pH of 8.5 to prevent unspecific labeling (33) and to ensure that even in the absence of Ca^{2+} the enzyme without Tg or metal fluoride bound resides predominantly in the *E*1 state rather than *E*2 (44). We were concerned that the enzyme-inhibitor complexes remained stable during photolabeling, and by studying the time course of reactivation following addition of Ca^{2+}, evidence was obtained that all five enzyme-inhibitor complexes were very stable under the photolabeling conditions, despite the high pH of the medium (supplemental Fig. S2).

The time dependence of photolabeling of expressed wild type Ca^{2+}-ATPase pre-equilibrated with or without inhibitor is shown in Fig. 1*A*. With the current irradiation setup, photolabeling proceeded at a rate of ~3 min^{-1} irrespective of the enzyme conformational state/inhibitor bound. The photolabeling rate of ~3 min^{-1} is comparable with the rate of photolysis of the azido group in TNP-$8N_3$-ATP of ~2 min^{-1}, determined using the same irradiation setup, *cf.* supplemental Fig. S4, implying that for Ca^{2+}-ATPase with or without bound fluoride complex or vanadate the rate-limiting step in the labeling reaction is the formation of the reactive nitrene (*cf.* Scheme 3). The subsequent chemical reaction between the nitrene of the photoactivated nucleotide and Lys^{492} of the Ca^{2+}-ATPase (Scheme 3) is likely much faster, given the typical short lifetime and high reactivity of nitrene intermediates (45, 46). Based on the time dependence of TNP-$8N_3$-ATP photolabeling of the Ca^{2+}-ATPase (Fig. 1*A*) as well as the time dependence of TNP-$8N_3$-ATP photolysis (supplemental Fig. S4), a pre-steady state irradiation time of 35 s was chosen for all subsequent photolabeling experiments.

The maximum levels of photolabeling (corresponding to saturation with photolabel) of the expressed wild type Ca^{2+}-ATPase as well as SR were ~3.5-fold higher in the *E*2·vanadate, *E*2·AlF, and *E*2·MgF states and ~1.7-fold higher in the *E*2·BeF state than in *E*2·Tg or *E*1 (Fig. 1). The labeling stoichiometry corresponding to the highest labeling levels indicated as 100% in Fig. 1 can be roughly estimated to be ~0.7 mol of label incorporated per mol of Ca^{2+}-ATPase present in the microsomal membrane, assuming that no label or protein is lost during gel electrophoresis. The higher maximum levels of photolabeling in the vanadate- and metal fluoride-complexed states as compared with *E*2·Tg or *E*1 do not result from additional labeling of other residues than Lys^{492}, because no labeling of the mutant

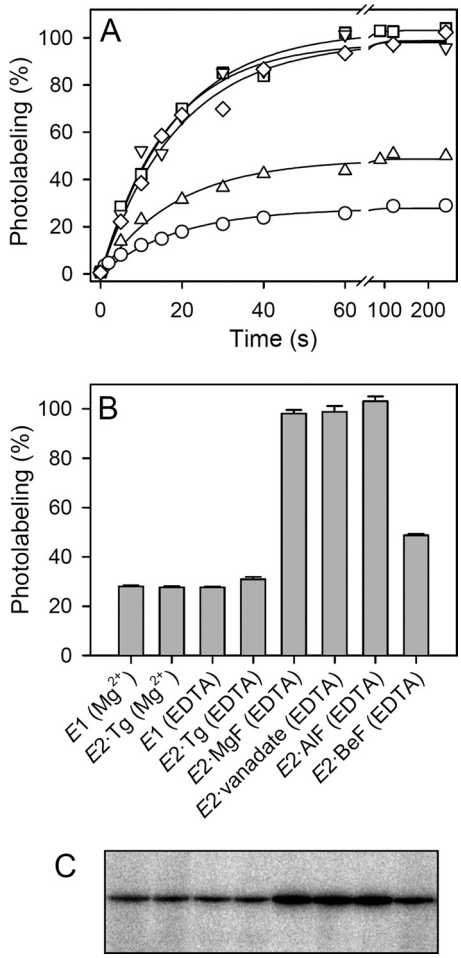

FIGURE 1. **Time dependence of TNP-$8N_3$-ATP photolabeling and photolabeling levels of Ca^{2+}-ATPase in various conformational states.** Microsomes containing expressed wild type Ca^{2+}-ATPase were pre-equilibrated with or without metal fluoride or vanadate, and subjected to TNP-$8N_3$-ATP photolabeling for various time intervals, as indicated on the *abscissa* in *panel A*, or for 60 s (*panel B*). The *symbols* in *panel A* are as follows: *circles*, *E*1 (Mg^{2+}); *triangles pointing downward*, *E*2·MgF; *diamonds*, *E*2·vanadate; *squares*, *E*2·AlF; *triangles pointing upward*, *E*2·BeF. In each case, the concentration of TNP-$8N_3$-ATP used was 3× the $K_{0.5}$ for TNP-$8N_3$-ATP (*cf.* Fig. 2). The labeling medium contained either $MgCl_2$ (with EGTA) or EDTA as indicated in *panel B* (for *panel A*, *E*1 was studied with Mg^{2+} present). The labeling level (in %), relative to the average of that obtained with *E*2·MgF, *E*2·vanadate, and *E*2·AlF, is in each panel indicated at the *ordinate*. *Panel C* shows a representative gel with lanes corresponding to the columns in the bar chart.

K492L was seen in any of the enzyme states examined (Table 1 and supplemental Fig. S5). Rather, the increased labeling levels may reflect a conformational change resulting in shortening of the interaction distance between Lys^{492} and the azido group of TNP-$8N_3$-ATP and/or desolvation of the intervening space thereby removing competing water molecules and increasing the nucleophilicity of the amino group, resulting in increased efficiency of the coupling reaction between Lys^{492} and the reactive nitrene of the photolabel following UV irradiation (*cf.* Scheme 3). Apart from this clue, little detail is known about the interactions of the photolabel in the various conformational states. Although competition of the photolabel with ATP for binding indicates that there is at least a partial overlap of binding sites, it is also clear from the difference in mutational effects on affinities for photolabel and ATP that the photolabel must bind rather differently from ATP (see below, compare Tables 1

TABLE 1

Affinity for TNP-8N_3-ATP of SR and expressed wild type Ca^{2+}-ATPase and mutants in various stabilized states

$K_{0.5}$ values for photolabeling derived from Figs. 2, 7, and supplemental Fig. S6 are indicated relative (in %) to that of the expressed wild type under the same conditions (for wild type the absolute $K_{0.5}$ value is shown). The S.E. is indicated with the number of experiments in parentheses.

	EDTA[a]					EGTA/Mg^{2+}[b]
	*E*2 (Tg)	*E*2·P_i (MgF)	*E*2·P (vanadate)	*E*2·P (AlF)	*E*2−P (BeF)	*E*1
Wild type	100 ± 14 (*n* = 4) (62 nM)	100 ± 12 (*n* = 6) (10.5 nM)	100 ± 10 (*n* = 8) (9.6 nM)	100 ± 9 (*n* = 9) (11.6 nM)	100 ± 14 (*n* = 7) (54 nM)	100 ± 18 (*n* = 5) (290 nM)
SR	84 ± 11 (*n* = 3)	90 ± 14 (*n* = 5)	74 ± 7 (*n* = 4)	69 ± 10 (*n* = 3)	83 ± 6 (*n* = 3)	89
R174A	331 ± 17 (*n* = 2)	269 ± 7 (*n* = 2)	251 ± 7 (*n* = 2)	255 ± 7 (*n* = 2)	795 ± 27 (*n* = 2)	73
R174E	536 ± 43 (*n* = 2)	1781 ± 171 (*n* = 2)	1735 ± 0 (*n* = 2)	878 ± 49 (*n* = 2)	1582 ± 340 (*n* = 2)	80
I188A	127 ± 1 (*n* = 2)	109 ± 20 (*n* = 2)	100 ± 16 (*n* = 2)	122 ± 18 (*n* = 2)	64 ± 18 (*n* = 2)	42
I188F	87 ± 5 (*n* = 2)	154 ± 16 (*n* = 2)	76 ± 5 (*n* = 2)	69 ± 6 (*n* = 2)	19 ± 2 (*n* = 2)	68
K205A	357 ± 2 (*n* = 2)	854 ± 196 (*n* = 2)	1131 ± 123 (*n* = 2)	1031 ± 9 (*n* = 2)	567 ± 6 (*n* = 2)	56
E439A	141 ± 6 (*n* = 2)	110 ± 6 (*n* = 2)	123 ± 11 (*n* = 2)	177 ± 11 (*n* = 3)	22 ± 3 (*n* = 2)	35
F487L	36 ± 5 (*n* = 2)	52 ± 15 (*n* = 2)	48 ± 5 *n* = 2)	60 ± 0 (*n* = 2)	19 ± 0 (*n* = 2)	43
F487S	90 ± 16 (*n* = 2)	89 ± 15 (*n* = 3)	101 ± 1 (*n* = 2)	81 ± 1 (*n* = 2)	88 ± 1 (*n* = 2)	25
R489L	965 ± 107 (*n* = 3)	116 ± 12 (*n* = 2)	108 ± 3 (*n* = 2)	120 ± 2 (*n* = 2)	702 ± 109 (*n* = 2)	85
K492L	No labeling	No labeling	No labeling	No labeling	No labeling	No labeling
R560L	311 ± 0 (*n* = 2)	77 ± 19 (*n* = 2)	98 ± 16 (*n* = 3)	64 ± 8 (*n* = 2)	138 ± 5 (*n* = 2)	1250
L562F	136 ± 17 (*n* = 2)	100 ± 4 (*n* = 2)	81 ± 15 (*n* = 2)	110 ± 20 (*n* = 2)	52 ± 8 (*n* = 2)	25
4Gi-46/47	151 ± 23 (*n* = 2)	83 ± 0 (*n* = 2)	96 ± 5 (*n* = 2)	106 ± 2 (*n* = 2)	83 ± 7 (*n* = 2)	96 ± 17 (*n* = 2)

[a] EDTA refers to the condition without free Mg^{2+} present described under "Experimental Procedures."
[b] EGTA/Mg^{2+} refers to the condition with free Mg^{2+} present (*E*1 state) described under "Experimental Procedures." Except in the case of mutant 4Gi-46/47, the data shown in this column have been published previously (16, 17, 33, 34) and are included for comparison.

TABLE 2

Affinity for ATP of SR and expressed wild type Ca^{2+}-ATPase and mutants in various stabilized states

K_D values derived from competitive inhibition of photolabeling by ATP (Figs. 2, 5, and 7) are indicated relative (in %) to that of the expressed wild type obtained under the same conditions (for wild type the absolute K_D value is shown). The S.E. is indicated with the number of experiments in parentheses.

	EDTA[a]					EGTA/Mg^{2+}[b]
	*E*2 (Tg)	*E*2·P_i (MgF)	*E*2·P (vanadate)	*E*2·P (AlF)	*E*2−P (BeF)	*E*1
Wild type	100 ± 9 (*n* = 8) (10.8 μM)	100 ± 19 (*n* = 5) (0.89 μM)	100 ± 9 (*n* = 4) (1.01 μM)	100 ± 7 (*n* = 7) (1.33 μM)	100 ± 7 (*n* = 6) (4.1 μM)	100 ± 5 (*n* = 4) (0.14 μM)
SR	96 ± 8 (*n* = 5)	90 ± 7 (*n* = 3)	81 ± 6 (*n* = 3)	52 ± 6 (*n* = 4)	60 ± 6 (*n* = 3)	78
R174A	316 ± 38 (*n* = 2)	256 ± 29 (*n* = 2)	224 ± 42 (*n* = 2)	256 ± 8 (*n* = 2)	1070 ± 61 (*n* = 2)	182
R174E	503 ± 4 (*n* = 2)	3445 ± 168 (*n* = 2)	2579 ± 272 (*n* = 2)	1157 ± 15 (*n* = 2)	4307 ± 964 (*n* = 3)	425
I188A	75 ± 1 (*n* = 2)	43 ± 4 (*n* = 2)	47 ± 4 (*n* = 2)	56 ± 6 (*n* = 2)	31 ± 4 (*n* = 2)	45
I188F	97 ± 17 (*n* = 3)	187 ± 12 (*n* = 2)	91 ± 2 (*n* = 2)	56 ± 0 (*n* = 2)	476 ± 68 (*n* = 2)	110
K205A	267 ± 2 (*n* = 2)	1147 ± 117 (*n* = 2)	1257 ± 10 (*n* = 2)	1198 ± 26 (*n* = 2)	249 ± 36 (*n* = 3)	139
E439A	78 ± 1 (*n* = 2)	195 ± 31 (*n* = 2)	237 ± 8 (*n* = 2)	631 ± 74 (*n* = 3)	32 ± 5 (*n* = 3)	235
F487L	1594 ± 121 (*n* = 2)	133 ± 10 (*n* = 2)	138 ± 0 (*n* = 2)	127 ± 17 (*n* = 2)	354 ± 10 (*n* = 2)	2,200
F487S	1219 ± 14 (*n* = 2)	1717 ± 450 (*n* = 4)	1294 ± 303 (*n* = 3)	1104 ± 53 (*n* = 2)	2309 ± 229 (*n* = 3)	>100,000
R489L	1896 ± 97 (*n* = 2)	252 ± 48 (*n* = 2)	285 ± 38 (*n* = 2)	203 ± 8 (*n* = 2)	1168 ± 283 (*n* = 2)	1600
K492L	Not feasible	Not feasible	Not feasible	Not feasible	Not feasible	Not feasible
R560L	3555 ± 23 (*n* = 2)	2019 ± 419 (*n* = 2)	1977 ± 356 (*n* = 3)	1172 ± 150 (*n* = 2)	3762 ± 369 (*n* = 3)	>100,000
L562F	213 ± 36 (*n* = 3)	67 ± 3 (*n* = 2)	64 ± 12 (*n* = 2)	106 ± 1 (*n* = 2)	132 ± 18 (*n* = 2)	6,900
4Gi-46/47	261 ± 62 (*n* = 2)	89 ± 10 (*n* = 2)	75 ± 1 (*n* = 2)	102 ± 5 (*n* = 2)	93 ± 17 (*n* = 2)	>100,000 (*n* = 4)

[a] EDTA refers to the condition without free Mg^{2+} present described under "Experimental Procedures."
[b] EGTA/Mg^{2+} refers to the condition with free Mg^{2+} present (*E*1 state) described under "Experimental Procedures." Except in the case of mutant 4Gi-46/47, the data shown in this column have been published previously (16, 17, 33, 34) and are included for comparison.

and 2, the difference is particularly striking for mutants F487S and R560L).

Nucleotide Affinity of Wild Type Ca^{2+}-ATPase in E2·Tg, E2·MgF, E2·Vanadate, E2·AlF, and E2·BeF States—We then proceeded to study the TNP-8N_3-ATP concentration dependence of photolabeling of SR and expressed wild type Ca^{2+}-ATPase in the *E*2·Tg, *E*2·MgF, *E*2·vanadate, *E*2·AlF, and *E*2·BeF states (Fig. 2, *left panels*). The TNP-8N_3-ATP affinity of the expressed wild type Ca^{2+}-ATPase with thapsigargin bound was 62 nM (Fig. 2, *upper left panel*, and Table 1).[4] A similar affinity of 54 nM (although, as noted above, with a 1.7-fold higher maximum labeling level) was obtained for the *E*2·BeF state of the expressed wild type. In contrast, the TNP-8N_3-ATP affinities of the *E*2·MgF, *E*2·vanadate, and *E*2·AlF states of the expressed wild type were significantly higher, in the 9–12 nM range (Table 1), possibly due to the same conformational change that results in the ~3.5-fold higher maximal labeling levels described above. In comparison, the affinity for TNP-8N_3-ATP of the uncomplexed wild type in the presence of Mg^{2+} (*E*1 state) was 290 nM (Table 1).[4] The TNP-8N_3-ATP affinities of SR with bound Tg, MgF, vanadate, AlF, and BeF were rather similar to

[4] In our previous studies of TNP-8N_3-ATP photolabeling of the Ca^{2+}-ATPase, [γ-^{32}P]TNP-8N_3-ATP synthesis and irradiation experiments were performed at the University of Cape Town. In the present study [γ-^{32}P]TNP-8N_3-ATP synthesis and irradiation experiments were carried out at Aarhus University. For unidentified reasons, the TNP-8N_3-ATP and ATP affinity constants measured in Aarhus with our new photolabeling setup were generally 2–3-fold lower (*i.e.* higher affinity) than those previously measured in Cape Town. For instance, under *E*1 conditions in the presence of Mg^{2+}, the affinities of the expressed wild type for TNP-8N_3-ATP and ATP measured in Aarhus were 0.29 and 0.14 μM (Tables 1 and 2), respectively, the previously published values being 0.79 and 0.51 μM, respectively. Similarly, in the *E*2·Tg state, the affinities of the expressed wild type for TNP-8N_3-ATP and ATP measured in Aarhus were 62 nM and 10.8 μM (Tables 1 and 2), respectively, the previously published values being 150 nM and 20 μM, respectively (16). We do not presently know the exact reason for the difference.

those obtained with the expressed wild type (compare Fig. 2, *upper left* and *lower left panels*).

Fig. 2, *right panels*, illustrates the inhibition by ATP of TNP-$8N_3$-ATP photolabeling, showing also that the ATP affinity of the *E2*·vanadate, *E2*·AlF, and *E2*·MgF forms of expressed wild type Ca^{2+}-ATPase or SR Ca^{2+}-ATPase is much higher (K_D ~1 μM) than that of *E2*·Tg (K_D 11 μM), although not nearly as high as the affinity of the *E*1 state (K_D 0.14 μM).[4] In *E2*·BeF, the affinity for ATP was of an intermediate magnitude (K_D 4 μM). These data are summarized in Table 2. The higher ATP affinity of the *E2*P transition state analogs *E2*·vanadate and *E2*·AlF, as compared with the *E2*P ground state analog, *E2*·BeF, and the *E2* dephosphoenzyme, makes it conceivable that stimulation of *E2*P dephosphorylation by ATP is accomplished by increasing the stability of the transition state of *E2*P dephosphorylation, thereby lowering the energy barrier for formation of the transition state. The binding of the modulatory ATP may lead to a more compact packing of the A-, P-, and N-domains and to an optimal positioning of Glu^{183} in the ^{181}TGES motif of the A-domain for coordinating the attacking water molecule during dephosphorylation (3–5) (*cf.* Fig. 3). In addition, stabilization of the product state *E2*·P_i, as evidenced by the high ATP affinity of the *E2*·MgF complex, could be of importance for the modulatory effect on the dephosphorylation.

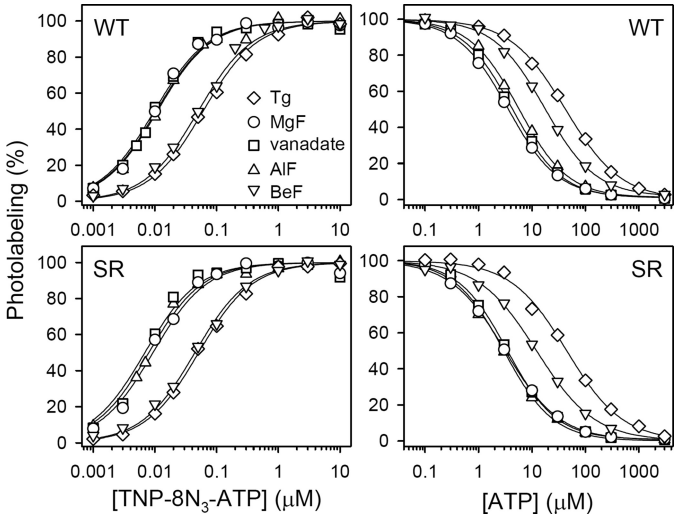

FIGURE 2. **TNP-$8N_3$-ATP (*left panels*) and ATP (*right panels*) concentration dependences of photolabeling of wild type Ca^{2+}-ATPase stabilized in the intermediate states occurring during *E2*P dephosphorylation.** Expressed wild type Ca^{2+}-ATPase (*upper panels*) or SR (*lower panels*) was incubated with Tg, MgF, vanadate, AlF, or BeF as described under "Experimental Procedures," and subjected to TNP-$8N_3$-ATP photolabeling at the indicated concentrations of TNP-$8N_3$-ATP without ATP (*left panels*), or at 3× the $K_{0.5}$ for TNP-$8N_3$-ATP with the indicated concentrations of ATP (*right panels*). In each case, the maximum level of specific labeling was defined as 100%. *Symbols* for all panels are indicated in the *upper left panel*.

Nucleotide Binding to E2·Tg·AlF—Thapsigargin has been widely applied in crystallization studies of the Ca^{2+}-ATPase either without (30, 47) or with additional inhibitors such as MgF (5), AlF (4, 48), or BeF (48). To address the issue whether thapsigargin binding influences the nucleotide affinity of the metal fluoride complex, we measured TNP-$8N_3$-ATP and ATP binding to enzymes complexed by both Tg and AlF (Fig. 4). SR vesicles were incubated under optimal conditions for forming the *E2*·AlF complex, followed by supplementation and further incubation with 1 μM Tg. Alternatively, incubation was first carried out with Tg and then with AlF. As seen in Fig. 4, the result was independent of which complex was formed first. The affinity of *E2*·Tg·AlF for TNP-$8N_3$-ATP was 17–18 nM, *i.e.* ~2-fold lower and ~3-fold higher than the TNP-$8N_3$-ATP

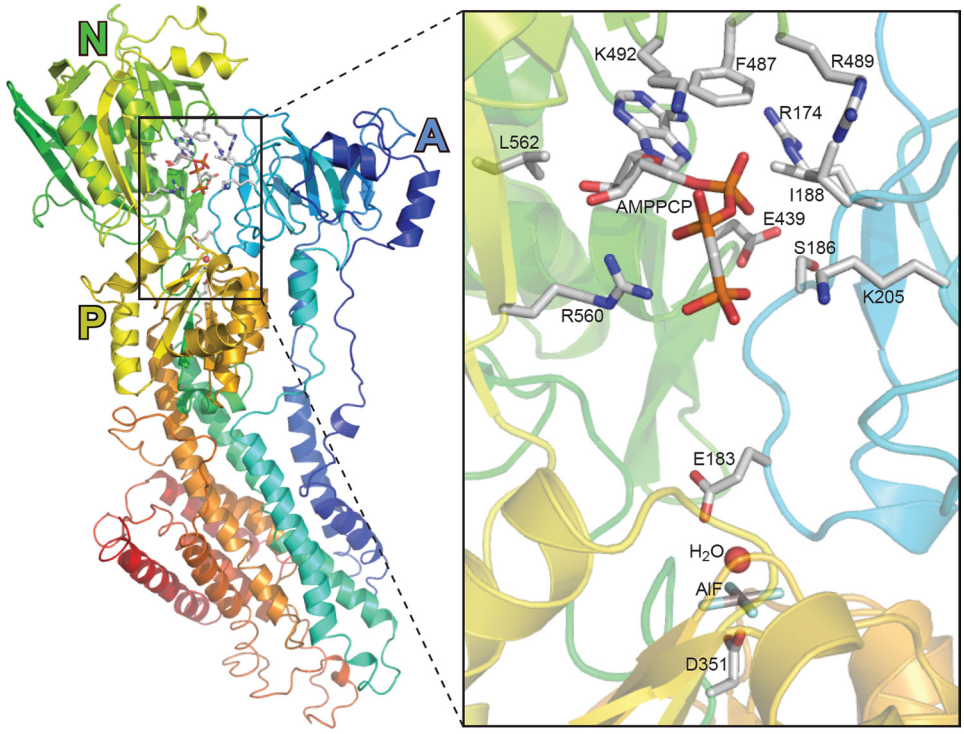

FIGURE 3. **Structural arrangement of the nucleotide binding site in Ca^{2+}-ATPase crystallized in the *E2*·AlF·AMPPCP state.** The Protein Data Bank accession code corresponding to the structure shown is 3B9R (26). Amino acid side chains are shown for residues discussed in the text. Carbon and aluminum atoms are shown in *gray*, nitrogen in *blue*, oxygen in *red*, phosphorous in *orange*, and fluoride in *cyan*.

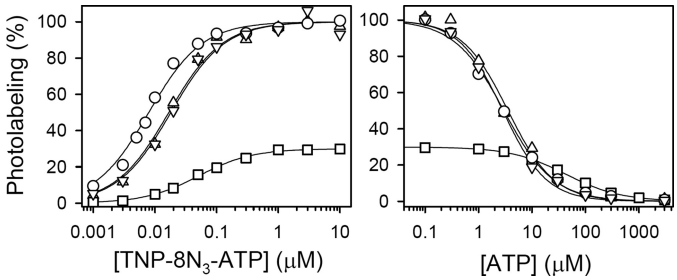

FIGURE 4. **TNP-$8N_3$-ATP (*left panel*) and ATP (*right panel*) concentration dependences of photolabeling of Ca^{2+}-ATPase in the *E2*·Tg·AlF state.** Formation of the *E2*·Tg·AlF state with SR was accomplished by first forming the *E2*·Tg state, followed by supplementation with $AlCl_3$, NaF, and $MgCl_2$ to final concentrations of 0.5, 2, and 0.2 mM, respectively (*triangles pointing downward*), or by first forming the *E2*·AlF state, followed by supplementation with 1 μM Tg (*triangles pointing upward*), and further incubation for 30 min at 25 °C. TNP-$8N_3$-ATP photolabeling was then carried out at the indicated concentrations of TNP-$8N_3$-ATP without ATP (*left panel*) or at 3× the $K_{0.5}$ for TNP-$8N_3$-ATP with the indicated concentrations of ATP (*right panel*). For comparison, results with SR in the *E2*·Tg (*squares*) and *E2*·AlF states (*circles*) (*cf.* Fig. 2) are included in the panels. In each case, the labeling level (in %) is shown relative to the labeling level of *E2*·AlF.

affinity of the *E2*·AlF and *E2*·Tg complexes, respectively (Fig. 4, *left panel*). The affinity of *E2*·Tg·AlF for ATP was on the other hand very similar to that of *E2*·AlF but 12- to 15-fold higher than that of *E2*·Tg (Fig. 4, *right panel*), implying that AlF binding dominates over Tg binding with respect to influencing the conformation of the ATP binding site in the *E2*·Tg·AlF complex. Also with respect to the maximal labeling levels seen in Fig. 4 did the *E2*·Tg·AlF complex resemble *E2*·AlF more than *E2*·Tg (*cf.* Fig. 1). Thus, the maximum labeling level of *E2*·Tg·AlF was ~3.5-fold higher than that of *E2*·Tg. It can be concluded that phosphorylation and nucleotide binding sites are fully flexible in the Tg-bound state, readily able to bind the AlF complex, and subsequently be photolabeled by TNP-$8N_3$-ATP with a $K_{0.5}$ for the photolabel, a $K_{0.5}$ for the inhibition by ATP of the photolabeling, and a maximal photolabeling level similar to that of the AlF-complexed, but Tg-free, enzyme. Hence, the inhibitory effect on catalysis of thapsigargin binding between transmembrane helixes M3, M5, and M7 (30) is a local effect in the membrane, leaving the cytoplasmic domains free to bind nucleotide and adopt the various conformations characteristic of the transitional states of *E*2P dephosphorylation.

ATP Affinity of Mutant Ca^{2+}-ATPases in E2·Tg, E2·MgF, E2·Vanadate, E2·AlF, and E2·BeF States—Studies of the ATP dependence of the rate of *E*2P dephosphorylation in mutants (16, 17, 24) have pinpointed certain residues as critical for ATP modulation of *E*2P dephosphorylation, including Glu^{439}, Phe^{487}, and Arg^{560} in the N-domain and Arg^{174}, Ile^{188}, and Lys^{205} in the A-domain (Fig. 3). To understand how the effect of ATP on *E*2P dephosphorylation is brought about, a critical question to answer for each of these residues is whether the residue is directly involved in binding of the modulatory nucleotide, or its role is instead associated with mediating the response to binding. By applying the photolabeling assay to determine the ATP affinity of the various states of the *E*2P dephosphorylation reaction sequence in mutants, it is possible to distinguish between mutational effects on ATP modulation caused by direct interference with ATP binding and effects caused by interference with the consequences of the binding. This analysis was carried out with a

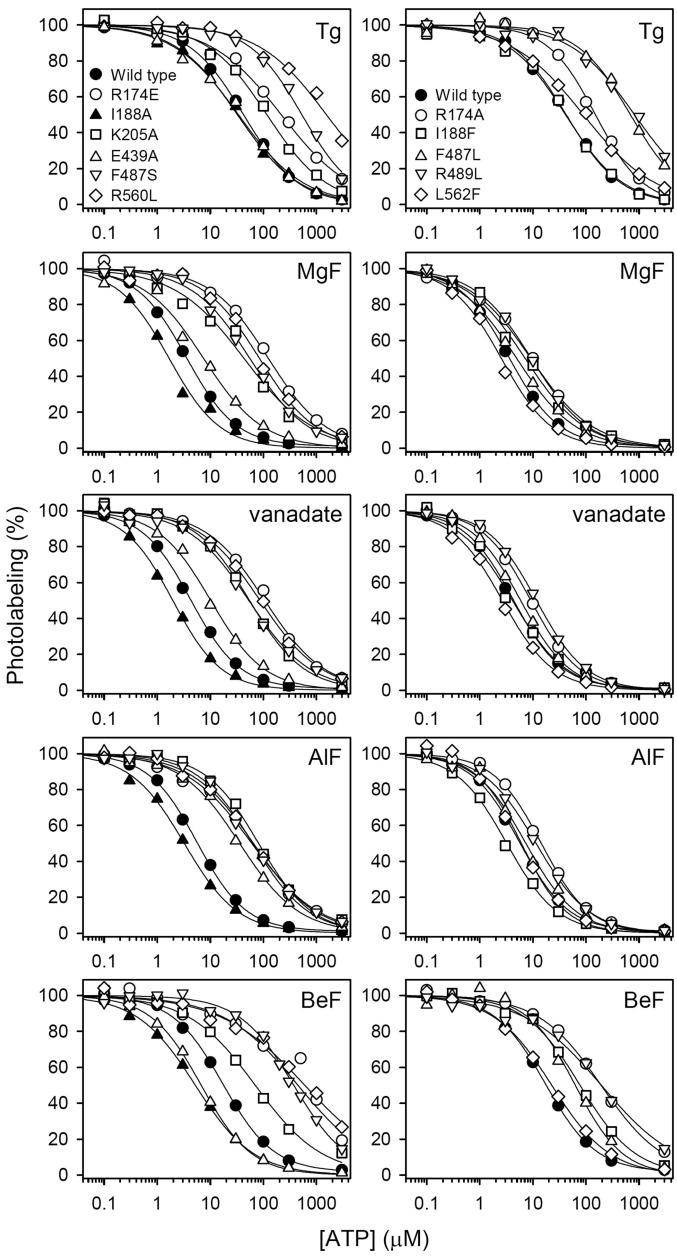

FIGURE 5. **ATP concentration dependences of photolabeling of Ca^{2+}-ATPase mutants stabilized in the intermediate states occurring during *E2*P dephosphorylation.** Expressed Ca^{2+}-ATPase was incubated with Tg, MgF, vanadate, AlF, or BeF as described under "Experimental Procedures," and subjected to TNP-$8N_3$-ATP photolabeling at 3× the $K_{0.5}$ for TNP-$8N_3$-ATP (the TNP-$8N_3$-ATP concentration dependences are shown in supplemental Fig. S6) in the presence of the indicated concentrations of ATP. In each case, the maximum level of specific labeling was defined as 100%. The affinity constants determined are listed in Table 2. Symbols for the five panels above each other are indicated in the *top panels*.

series of mutants previously shown to be defective in ATP modulation of *E*2P dephosphorylation as observed in functional studies (R174A, R174E, I188A, I188F, K205A, E439A, F487S, and R560L, *cf.* Refs. 16 and 17) and with selected mutants previously found defective in ATP binding at the catalytic site in the *E*1 conformation (F487S, F487L, R489L, R560L and L562F, *cf.* Refs. 33 and 34). The binding data are displayed in Fig. 5 for ATP and under supplemental Fig. S6 for TNP-$8N_3$-ATP, and the resulting affinity constants are listed in Tables 1 and 2.

Mutants with alterations to N-domain residues Phe^{487}, Arg^{489}, Arg^{560}, and Leu^{562} (*cf.* Fig. 3) were previously shown to be severely defective with respect to ATP binding at the catalytic site in the *E*1 conformation (33, 34) (Table 2, *right column*). In functional studies mutations F487S and R560L were, furthermore, found to reduce the apparent affinity for ATP modulation of *E*2P dephosphorylation as much as >50- and 30-fold, respectively (16), which on the basis of the binding data in Fig. 5 and Table 2 can be ascribed to a deficiency of binding of the modulatory ATP throughout the *E*2P dephosphorylation reaction sequence. Hence, ATP binding affinity in the five *E*2/*E*2P states was reduced 11–23-fold for mutant F487S and 12–38-fold for mutant R560L, relative to wild type. Phe^{487} and Arg^{560} are in close proximity to the nucleotide in the *E*1·AMPPCP, *E*2·Tg·AMPPCP, *E*2·MgF·AMPPCP/ATP/ADP, and *E*2·AlF·AMPPCP crystal structures, with Phe^{487} apparently interacting with the adenine ring and Arg^{560} with the ribose and/or the β-phosphate (5, 26, 47–50), and the present data support the notion that the catalytic ATP binding site in the *E*1 state and the modulatory ATP binding site responsible for stimulation of *E*2P dephosphorylation are overlapping. Mutation F487L, retaining the bulk and hydrophobicity of the side chain, was, however, much less detrimental to ATP binding than F487S, in the *E*2P-like analog states stabilized with MgF, vanadate, AlF, and BeF. Hence, a wild type-like affinity for ATP was seen for mutant F487L in *E*2·MgF, *E*2·vanadate, and *E*2·AlF states, and in *E*2·BeF the ATP affinity was only moderately (3.5-fold) reduced. The effect of the F487L mutation was much more pronounced in the *E*1 and *E*2·Tg states (22- and 16-fold reduction of ATP affinity, respectively, *cf.* Table 2). In most of the crystal structures with bound nucleotide the adenine ring is interposed between Phe^{487} and Leu^{562}. In the Ca_2E1 state, the aromatic ring of the phenylalanine side chain is nearly parallel to the adenine ring, indicating a π-stacking interaction that explains the marked effect of the leucine substitution in this state. In the *E*2·MgF and *E*2·AlF crystal structures the phenylalanine and adenine rings are more angled toward each other, suggesting less efficient π-stacking, which might be the reason that despite the lack of aromaticity the leucine is able to substitute quite well for phenylalanine in these states. In the *E*2·Tg state, however, mutation F487L was just as detrimental to ATP binding as in *E*1, despite a non-parallel orientation of the phenylalanine ring and the adenine ring in the *E*2·Tg·AMPPCP crystal structures, thus implying that positioning of the adenine ring in the native enzyme in the *E*2·Tg state differs somewhat from that seen in the *E*2·Tg·AMPPCP crystal structures.

Mutation L562F was previously shown to reduce MgATP affinity of *E*1 69-fold (34) but appears much less distorting in the intermediate *E*2/*E*2P states of *E*2P dephosphorylation, the most marked effect being a 2-fold reduced ATP affinity in *E*2·Tg (Table 2), which is somewhat surprising, because the Leu^{562} side chain occupies almost exactly the same position relative to the nucleotide in the Ca_2E1·AMPPCP, *E*2·Tg·AMPPCP, *E*2·MgF·AMPPCP/ATP/ADP, and *E*2·AlF·AMPPCP crystal structures, being located 3.2–3.7 Å from the ribose and 3.3–4.9 Å from the adenine ring (26, 47–50). It is possible that because of a higher mobility of the bound ATP in the *E*2/*E*2P states, as reflected by the lower ATP affinity of wild type *E*2/*E*2P states (K_D values in the 1–11 μM range; Table 2) compared with that of *E*1 (K_D = 0.14 μM; Table 2), the bound nucleotide in the *E*2/*E*2P states can be correctly positioned by any large hydrophobic side chain replacing Leu^{562}. This would not be feasible in the very tight enzyme-nucleotide complex normally seen for *E*1, where a phenylalanine side chain cannot be accommodated in place of the leucine without destabilization of the complex. Accordingly, the affinity of the *E*1 state of L562F for MgATP (~10 μM) is a bit lower than the affinity of the *E*2P states of L562F for ATP (0.5–5 μM) (Table 2).

Mutation R489L was equally detrimental to ATP binding in *E*2·Tg and *E*2·BeF (19- and 12-fold reduction of affinity, respectively, relative to wild type) as to MgATP binding in *E*1 (16-fold reduction), whereas the effect was much less pronounced for *E*2·MgF, *E*2·vanadate, and *E*2·AlF (2–3-fold reduced ATP affinities, relative to wild type) (Table 2). This finding provides additional evidence that ATP is bound differently in the *E*2 dephosphoenzyme and the *E*2P ground state compared with the *E*2P transition and product states. The minor effects seen for the *E*2P transition state and product state analogs accord with the crystal structures of *E*2·AlF·AMPPCP and *E*2·MgF·AMPPCP/ATP/ADP, where the distance between the Arg^{489} side chain guanidinium group and the nucleotide ribose-OH is somewhat larger (4–6 Å) compared with the ~3 Å seen for the various Ca_2E1 crystals. In the *E*2·Tg·AMPPCP crystal structures the corresponding distance is 5.2 Å, again indicating that details of the positioning of the nucleotide differ somewhat from the native enzyme in the *E*2·Tg state, where Arg^{489} according to our result is an important interaction partner. Because the *E*2·BeF crystal structures (26, 48) do not contain bound nucleotide, there is so far no structural correlation of the marked effect of the R489L mutation on the ATP affinity of *E*2·BeF.

The A-domain residues Arg^{174}, Ile^{188}, and Lys^{205} are not involved in nucleotide binding in the *E*1 conformation, but were in our previous functional studies identified as critical for the ATP-induced acceleration of *E*2P dephosphorylation (17). The Arg^{174} side chain is rather close (~4 Å) to the adenine ring of the nucleotide in the product state (*E*2·MgF·AMPPCP/ATP/ADP) and transition state (*E*2·AlF·AMPPCP) (Fig. 3) analog crystal structures (5, 26, 49), whereas in the *E*2·Tg·AMPPCP crystal structure the bound nucleotide is too far away from Arg^{174} for any direct interaction (47). Substitution of Arg^{174} with alanine or glutamate leads to reduced apparent affinity for ATP modulation of *E*2P dephosphorylation, most markedly for R174E, in which the charge of the side chain is reversed (17). PP_i (pyrophosphate) was on the other hand found effective in stimulating dephosphorylation of mutant R174A with an affinity similar to that seen for the wild type, although the affinity of R174E for PP_i was reduced (17). Assuming that PP_i binds at the same site as modulatory ATP, mimicking the effect of the β- and γ-phosphates of ATP, the functional data would suggest that the role of Arg^{174} in ATP modulation of *E*2P dephosphorylation is associated primarily with binding of the adenosine part of the nucleotide and not the mechanism of mediating the effect of binding. The present binding data support this concept by showing that mutation R174A reduces the affinity for ATP as much as 11-fold in the *E*2P ground state (*E*2·BeF) and

~3-fold in the other *E*2/*E*2P-like analog states, and that R174E reduces the ATP affinity markedly (12–43-fold) in the four *E*2P-like analog states (Fig. 5 and Table 2). The more pronounced effect of replacement with glutamate, having a negatively charged side chain, may be a consequence of electrostatic repulsion of the phosphates of the ATP molecule (*cf.* Fig. 3).

Our previous functional analysis (17), furthermore, showed that stimulation by ATP of *E*2P dephosphorylation was completely abolished in mutant I188A, whereas I188F displayed a minor, 2-fold reduction of the apparent affinity for the modulation by ATP of *E*2P dephosphorylation. Because of the 3–5-Å proximity of the Ile^{188} side chain to the α-phosphate or adenine ring of the nucleotide in *E*2·MgF·ADP and *E*2·AlF·AMPPCP crystal structures (Fig. 3), one might have expected Ile^{188} to be directly involved in ATP binding during *E*2P dephosphorylation, which might explain the marked effect of mutation I188A on ATP modulation (17). The present binding analysis showed, however, that contrary to the expected lowering of affinity, the I188A mutation actually causes a significant 2–3-fold increase of ATP affinity in the four *E*2P-like analog states (Table 2, the corresponding K_D values are 0.4–1.3 μM), suggesting that in fact the larger side chain of isoleucine present in the wild type is a little disturbing to the binding of the nucleotide, the alanine of the mutant accommodating the nucleotide better. In this light, the complete absence of ATP modulation of dephosphorylation of *E*2P in I188A (Fig. 5 of Ref. 17) provides a clear indication of a mechanistic role of Ile^{188} in mediating the stimulating effect of ATP on *E*2P dephosphorylation. Ile^{188} is located at the start of the loop containing the TGES motif with Glu^{183}, and a slight clash between Ile^{188} and the nucleotide might be instrumental in moving Glu^{183} to the optimal position for catalyzing dephosphorylation. Because of the shorter side chain, alanine would not be able to fulfill this role, whereas the larger phenylalanine would (the efficiency of modulation is actually higher for I188F than for the wild type, see Table 3 in Ref. 17).

Mutants K205A and E439A are both modulated by ATP in a rather anomalous way, displaying inhibition rather than stimulation of *E*2P dephosphorylation by ATP (16, 17). This is illustrated for mutant E439A in Fig. 6, where more data points have been included than previously (16), showing inhibition between 0.2 and 5 mM ATP with a $K_{0.5}$ for inhibition of 3.1 mM. In comparison, wild type is stimulated by ATP with a $K_{0.5}$ of 34 μM. Phosphoenzyme decay curves for mutant E439A at various ATP concentrations are shown under supplemental Fig. S7. Detailed inhibition data for mutant K205A obtained in the same way were previously shown in Fig. 5 of Ref. 17. In the *E*2·MgF·AMPPCP/ATP/ADP and *E*2·AlF·AMPPCP (Fig. 3) crystal structures the side chain of Lys^{205} in the A-domain is close (3–4 Å) to the β- and γ-phosphates of the nucleotide, whereas the side chain of Glu^{439} in the N-domain is further away from the nucleotide (5–7 Å distant from the adenine ring). Indeed, the role of Glu^{439} in ATP modulation of *E*2P dephosphorylation is likely to be of an indirect nature, relating to an interdomain hydrogen bond between Glu^{439} and A-domain residue Ser^{186}, *cf.* Fig. 3 (16, 24), rather than to direct interaction with the modulatory nucleotide. The binding data in Fig. 5 provide a tentative explanation of the anomalous inhibitory effect

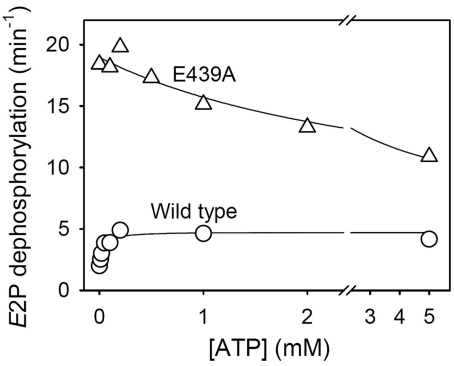

FIGURE 6. **ATP dependence of the rate of dephosphorylation of E_2P for mutant E439A.** Dephosphorylation of the phosphoenzyme formed in the presence of $^{32}P_i$ was followed at various ATP concentrations at pH 7.0 in the absence of Mg^{2+} as described under "Experimental Procedures." Examples of the decay curves are shown under supplemental Fig. S7. The dephosphorylation rate constants are shown here as a function of the ATP concentration. The parameters derived by fitting a hyperbolic function as described under "Experimental Procedures" are as follows (in each case, the total number of data points included in the fit is indicated in parentheses): wild type, $K_{0.5}$ = 34 ± 9 μM, k_0 = 2.0 min^{-1}, k_{max} = 4.7 min^{-1} (n = 22); E439A, $K_{0.5}$ = 3115 ± 2171 μM, k_0 = 19.0 min^{-1}, k_{max} = 5.6 min^{-1} (n = 19).

of ATP seen for K205A and E439A. The K_D values for ATP binding are for K205A, 10.2 μM in *E*2·BeF, 15.9 μM in *E*2·AlF, and 12.7 μM in *E*2·vanadate; and for E439A, 1.3 μM in *E*2·BeF, 8.4 μM in *E*2·AlF, and 2.4 μM in *E*2·vanadate, which should be compared with the wild type affinity constants of 4.1 μM in *E*2·BeF, 1.3 μM in *E*2·AlF, and 1 μM in *E*2·vanadate. Hence, for both mutants the ATP affinity is higher (*i.e.* K_D lower) in the ground state (*E*2·BeF) of *E*2P compared with the transition state (*E*2·AlF and *E*2·vanadate). This is contrary to the situation seen with wild type and all the other mutants studied here, where the ATP affinity of *E*2·BeF is lower than that of *E*2·AlF and *E*2·vanadate. Thus, whereas the nucleotide increases stability of the *E*2P transition state relative to the *E*2P ground state in the wild type, and consequently stimulates dephosphorylation, the opposite takes place in K205A and E439A, with the nucleotide instead increasing stability of the ground state relative to the transition state, thereby inhibiting dephosphorylation.

Nucleotide Affinity of the Stable Ca_2E2P State of Mutant 4Gi-46/47—For wild type Ca^{2+}-ATPase, the conformational transition of the phosphoenzyme, $Ca_2E1P \rightarrow Ca_2E2P$, is a rate-limiting step of the overall pump cycle, and is succeeded by rapid dissociation of the two Ca^{2+} ions from lumenally exposed Ca^{2+} sites to the endoplasmic reticulum lumen, thus forming the Ca^{2+}-free *E*2P ground state (*cf.* Scheme 1). The Ca_2E2P state is thought to be an unstable and short-lived intermediate that cannot be readily isolated. However, elongation of the A-M1 linker between the A-domain and transmembrane helix M1 by insertion of four glycines between Gly^{46} and Lys^{47} (mutant "4Gi-46/47") has been shown to result in an extremely stable Ca_2E2P state (31), in which the A-domain seems to have rotated horizontally from its position in the Ca_2E1P state, whereas the inclining (vertical) motion of the top part of transmembrane helix M2 and the A- and P-domains has yet to take place to reach the structure corresponding to the Ca^{2+}-free *E*2P ground state (32). It is then relevant to ask whether the latter conformational change also affects the nucleotide site, or the modulatory ATP binding site of *E*2P has already been

assembled from the gathering of the A-, P-, and N-domains, before the vertical tilt occurs.

To determine the nucleotide affinity of the stable Ca_2E2P state of mutant 4Gi-46/47, phosphorylation of Ca^{2+}-free *E*2 from the mutant was carried out with inorganic phosphate, followed by supplementation of the microsomes with an excess amount of Ca^{2+} to saturate the lumenal Ca^{2+} sites. These experiments were carried out in the presence of the Ca^{2+} ionophore A23187 to allow Ca^{2+} access to the lumenal side of the microsomal vesicles. The data under supplemental Fig. S8 confirm the high stability of the phosphoenzyme accumulated with mutant 4Gi-46/47 under the buffer conditions used in the photolabeling assay. The TNP-$8N_3$-ATP and ATP binding data obtained with the Ca_2E2P state of mutant 4Gi-46/47 are shown in Fig. 7*A*. For comparison, we furthermore, measured the TNP-$8N_3$-ATP and ATP affinities of mutant 4Gi-46/47 in the Tg-, MgF-, vanadate-, AlF-, and BeF-complexed states (Fig. 7*A*), as well as the TNP-$8N_3$-ATP and ATP affinities under *E*1 conditions in the absence of Ca^{2+} (Fig. 7*B*).

As shown in Fig. 7*A*, the Ca_2E2P state of mutant 4Gi-46/47 binds TNP-$8N_3$-ATP and ATP with affinities that do not differ significantly from those of the Ca^{2+}-free *E*2·BeF state of the mutant, implying that any conformational change taking place during the transition to the Ca^{2+}-free *E*2P ground state does not affect the nucleotide binding site. Furthermore, there was no marked difference between nucleotide affinities of wild type and mutant 4Gi-46/47 in any of the four *E*2P-like analog states stabilized with MgF, vanadate, AlF, and BeF, suggesting that the mutation does not disturb conformation of the *E*2P ground state, transition state, or product state appreciably, in accordance with the wild type-like rate of *E*2P dephosphorylation of the mutant (31).

Under *E*1 conditions mutant 4Gi-46/47 also displayed an affinity for TNP-$8N_3$-ATP very similar to that of wild type (Fig. 7*B*, *left panel*). Surprisingly, however, under these conditions the ATP affinity of mutant 4Gi-46/47 was reduced by more than 3 orders of magnitude, relative to wild type (*right panel* of Fig. 7*B*). To assess whether this effect of the 4Gi-46/47 mutation was caused by the absence of Ca^{2+} in the photolabeling medium (needed to prevent phosphorylation during labeling), we measured ATP dependence of phosphorylation of the Ca^{2+}-saturated *E*1 from [γ-^{32}P]ATP. As seen in Fig. 7*C*, the apparent affinity for ATP obtained with 4Gi-46/47 in the phosphorylation assay differed only 2-fold from that of the wild type enzyme. A possible explanation of these findings is that increased flexibility of the lengthened A-M1 linker in the mutant leads to detachment of the A-, P-, and N-domain interactions, resulting in stabilization in the absence of Ca^{2+} of an open structure similar to that seen in the crystal structure of the nucleotide-free Ca_2E1 state (51). In such a state, only the N-domain would be expected to contribute to nucleotide binding, as opposed to tight packing of the nucleotide between the N- and P-domains seen in the Ca_2E1·AMPPCP state (50). In accordance with this hypothesis, the ATP affinity of expressed N-domain from Ca^{2+}-ATPase or Na^+,K^+-ATPase is in the millimolar range (52–54), rather than the typical submicromolar/micromolar affinity range of the intact enzymes. The wild type-like high affinity of mutant 4Gi-46/47 for TNP-$8N_3$-ATP may

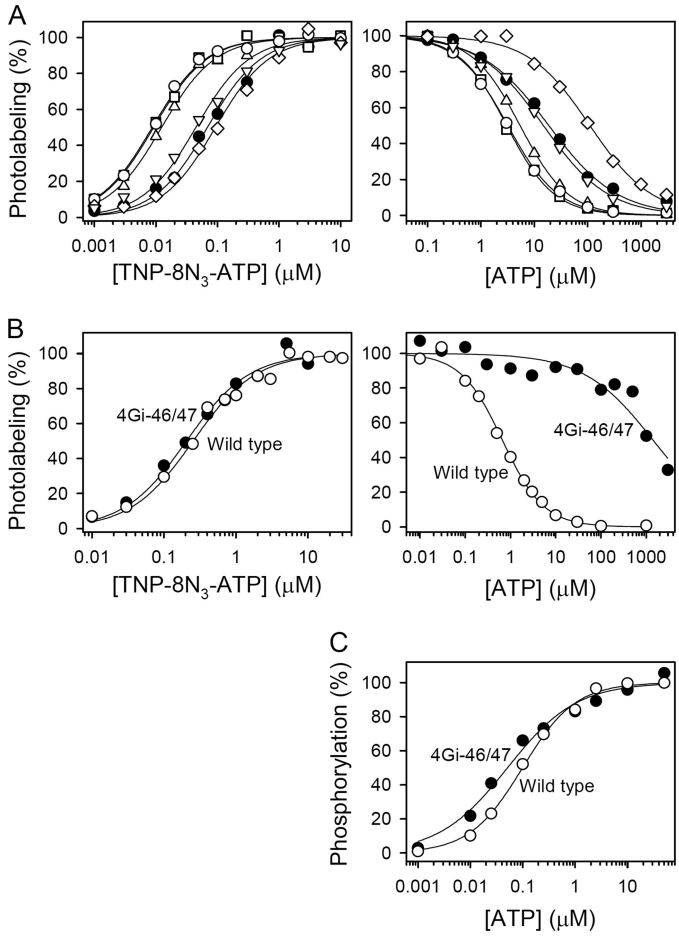

FIGURE 7. **Nucleotide binding properties of mutant 4Gi-46/47 in (*A*) *E*2·Tg, *E*2·MgF, *E*2·vanadate, *E*2·AlF, *E*2·BeF, and Ca_2E2P states, (*B*) *E*1 state, and (*C*) Ca_2E1 state.** *A*, TNP-$8N_3$-ATP (*left panels*) and ATP (*right panels*) concentration dependences of photolabeling of mutant 4Gi-46/47 in *E*2·Tg (*diamonds*), *E*2·MgF (*open circles*), *E*2·vanadate (*squares*), *E*2·AlF (*triangles pointing upward*), *E*2·BeF (*triangles pointing downward*), and Ca_2E2P (*closed circles*) states. Photolabeling was carried out as for Figs. 2, 5, and supplemental Fig. S6. The complexed state of mutant 4Gi-46/47 at the concentrations of metal fluoride, thapsigargin, or vanadate applied is confirmed by the results shown under supplemental Table S1 and Fig. S1. The Ca_2E2P state of mutant 4Gi-46/47 was formed by first phosphorylating the enzyme with inorganic phosphate and then adding a high concentration of Ca^{2+} to saturate the lumenal low affinity Ca^{2+} sites (see "Experimental Procedures"). The results of supplemental Fig. S8 confirm the high stability of the phosphoenzyme accumulated with mutant 4Gi-46/47 under the conditions used in the photolabeling assay. The nucleotide affinity constants obtained with mutant 4Gi-46/47 in Tg, MgF, vanadate, AlF, and BeF are listed in Tables 1 and 2, and those obtained with the Ca_2E2P state are as follows: $K_{0.5}$ (TNP-$8N_3$-ATP) = 69 ± 3 nM (n = 3); $K_{D(ATP)}$ = 4.6 ± 0.5 μM (n = 3). *B*, TNP-$8N_3$-ATP (*left panels*) and ATP (*right panels*) concentration dependence of photolabeling of wild type and mutant 4Gi-46/47 in the *E*1 state (Mg^{2+} present). The affinity constants obtained are listed in Tables 1 and 2, respectively. *C*, ATP concentration dependence of phosphorylation from [γ-^{32}P]ATP. The maximum phosphorylation level was taken as 100%. The following affinity constants were obtained: wild type, $K_{0.5}$ = 99 ± 6 nM (n = 5); 4Gi-46/47, $K_{0.5}$ = 51 ± 8 nM (n = 2).

then suggest that the N-domain generally is the only critical contributor to the binding of the photolabel, thus again illustrating the notion that the photolabel binds in a way rather different from that of ATP, although the binding sites overlap.

Conclusions—By applying the TNP-$8N_3$-ATP Lys^{492} photolabeling method (20, 33, 34) we have measured nucleotide binding to the various intermediate states occurring during *E*2P dephosphorylation of wild type and mutant Ca^{2+}-ATPases.

The distinct ATP affinities determined for these states in the wild type Ca^{2+}-ATPase suggest a certain degree of flexibility of the modulatory ATP site during *E*2P dephosphorylation, with a pronounced tightening of the enzyme-nucleotide interaction going from the *E*2P ground state to the transition state, perpetuation of this tight interaction further into the product state, and then loosening up the site again going into the *E*2 dephosphoenzyme. Hence, on the basis of the present results the acceleration of dephosphorylation by ATP can be understood in terms of stabilization by ATP binding of the transition and product states in the dephosphorylation reaction. Among the mutations studied here F487S, R560L, and R174A/E interfere with binding of the modulatory nucleotide, whereas I188A interferes mechanistically, possibly disrupting the effect of ATP binding on the optimal positioning of Glu^{183} for catalysis. The anomalous inhibition of *E*2P dephosphorylation by ATP seen for mutants K205A and E439A is caused by a reversal of the stabilities of the *E*2P ground and transition states. The present results fully support a model in which the adenine always slots into the gap between Phe^{487} and Leu^{562}, whether the ATP is phosphorylating the Ca_2E1 form or modulating *E*2P dephosphorylation, and then the rest of the ATP molecule stretches or folds, as is energetically best depending on domain positions, rather like an anchor and chain.

Acknowledgments—We thank Lene Jacobsen and Karin Kracht for expert technical assistance, Dr. Anne Nyholm Holdensen for supplying the cDNA encoding mutant 4Gi-46/47, and Dr. Philippe Champeil (Saclay, France) for generously donating the SR vesicles.

REFERENCES

1. Toyoshima, C. (2009) *Biochim. Biophys. Acta* **1793,** 941–946
2. Møller, J. V., Olesen, C., Winther, A. M., and Nissen, P. (2010) *Q. Rev. Biophys.* **43,** 501–566
3. Clausen, J. D., Vilsen, B., McIntosh, D. B., Einholm, A. P., and Andersen, J. P. (2004) *Proc. Natl. Acad. Sci. U.S.A.* **101,** 2776–2781
4. Olesen, C., Sørensen, T. L., Nielsen, R. C., Møller, J. V., and Nissen, P. (2004) *Science* **306,** 2251–2255
5. Toyoshima, C., Nomura, H., and Tsuda, T. (2004) *Nature* **432,** 361–368
6. Scofano, H. M., Vieyra, A., and de Meis, L. (1979) *J. Biol. Chem.* **254,** 10227–10231
7. Wakabayashi, S., and Shigekawa, M. (1990) *Biochemistry* **29,** 7309–7318
8. McIntosh, D. B., and Boyer, P. D. (1983) *Biochemistry* **22,** 2867–2875
9. Wakabayashi, S., Ogurusu, T., and Shigekawa, M. (1986) *J. Biol. Chem.* **261,** 9762–9769
10. Champeil, P., and Guillain, F. (1986) *Biochemistry* **25,** 7623–7633
11. Bodley, A. L., and Jencks, W. P. (1987) *J. Biol. Chem.* **262,** 13997–14004
12. Shigekawa, M., and Dougherty, J. P. (1978) *J. Biol. Chem.* **253,** 1451–1457
13. Ariki, M., and Boyer, P. D. (1980) *Biochemistry* **19,** 2001–2004
14. Champeil, P., Riollet, S., Orlowski, S., Guillain, F., Seebregts, C. J., and McIntosh, D. B. (1988) *J. Biol. Chem.* **263,** 12288–12294
15. Andersen, J. P., and Møller, J. V. (1985) *Biochim. Biophys. Acta* **815,** 9–15
16. Clausen, J. D., McIntosh, D. B., Anthonisen, A. N., Woolley, D. G., Vilsen, B., and Andersen, J. P. (2007) *J. Biol. Chem.* **282,** 20686–20697
17. Clausen, J. D., McIntosh, D. B., Woolley, D. G., and Andersen, J. P. (2008) *J. Biol. Chem.* **283,** 35703–35714
18. Cable, M. B., Feher, J. J., and Briggs, F. N. (1985) *Biochemistry* **24,** 5612–5619
19. Bishop, J. E., Al-Shawi, M. K., and Inesi, G. (1987) *J. Biol. Chem.* **262,** 4658–4663
20. Seebregts, C. J., and McIntosh, D. B. (1989) *J. Biol. Chem.* **264,** 2043–2052
21. Coll, R. J., and Murphy, A. J. (1991) *Biochemistry* **30,** 1456–1461
22. Suzuki, H., Kubota, T., Kubo, K., and Kanazawa, T. (1990) *Biochemistry* **29,** 7040–7045
23. Reynolds, J. A., Johnson, E. A., and Tanford, C. (1985) *Proc. Natl. Acad. Sci. U.S.A.* **82,** 3658–3661
24. Liu, X., Daiho, T., Yamasaki, K., Wang, G., Danko, S., and Suzuki, H. (2009) *J. Biol. Chem.* **284,** 25190–25198
25. Danko, S., Yamasaki, K., Daiho, T., and Suzuki, H. (2004) *J. Biol. Chem.* **279,** 14991–14998
26. Olesen, C., Picard, M., Winther, A. M., Gyrup, C., Morth, J. P., Oxvig, C., Møller, J. V., and Nissen, P. (2007) *Nature* **450,** 1036–1042
27. Cantley, L. C., Jr., Cantley, L. G., and Josephson, L. (1978) *J. Biol. Chem.* **253,** 7361–7368
28. Pick, U. (1982) *J. Biol. Chem.* **257,** 6111–6119
29. Sagara, Y., Wade, J. B., and Inesi, G. (1992) *J. Biol. Chem.* **267,** 1286–1292
30. Toyoshima, C., and Nomura, H. (2002) *Nature* **418,** 605–611
31. Daiho, T., Yamasaki, K., Danko, S., and Suzuki, H. (2007) *J. Biol. Chem.* **282,** 34429–34447
32. Daiho, T., Danko, S., Yamasaki, K., and Suzuki, H. (2010) *J. Biol. Chem.* **285,** 24538–24547
33. McIntosh, D. B., Woolley, D. G., Vilsen, B., and Andersen, J. P. (1996) *J. Biol. Chem.* **271,** 25778–25789
34. Clausen, J. D., McIntosh, D. B., Vilsen, B., Woolley, D. G., and Andersen, J. P. (2003) *J. Biol. Chem.* **278,** 20245–20258
35. Clausen, J. D., and Andersen, J. P. (2010) *J. Biol. Chem.* **285,** 20780–20792
36. Kaufman, R. J., Davies, M. V., Pathak, V. K., and Hershey, J. W. (1989) *Mol. Cell. Biol.* **9,** 946–958
37. Chen, C., and Okayama, H. (1987) *Mol. Cell. Biol.* **7,** 2745–2752
38. Maruyama, K., and MacLennan, D. H. (1988) *Proc. Natl. Acad. Sci. U.S.A.* **85,** 3314–3318
39. Champeil, P., Büschlen-Boucly, S., Bastide, F., and Gary-Bobo, C. (1978) *J. Biol. Chem.* **253,** 1179–1186
40. Champeil, P., Guillain, F., Vénien, C., and Gingold, M. P. (1985) *Biochemistry* **24,** 69–81
41. Vilsen, B., Andersen, J. P., and MacLennan, D. H. (1991) *J. Biol. Chem.* **266,** 16157–16164
42. Sorensen, T., Vilsen, B., and Andersen, J. P. (1997) *J. Biol. Chem.* **272,** 30244–30253
43. Vilsen, B., Andersen, J. P., Clarke, D. M., and MacLennan, D. H. (1989) *J. Biol. Chem.* **264,** 21024–21030
44. Forge, V., Mintz, E., and Guillain, F. (1993) *J. Biol. Chem.* **268,** 10953–10960
45. Chowdhry, V., and Westheimer, F. H. (1979) *Annu. Rev. Biochem.* **48,** 293–325
46. Kotzyba-Hibert, F., Kapfer, I., and Goeldner, M. (1995) *Angew. Chem. Int. Ed. Engl.* **34,** 1296–1312
47. Jensen, A. M., Sørensen, T. L., Olesen, C., Møller, J. V., and Nissen, P. (2006) *EMBO J.* **25,** 2305–2314
48. Toyoshima, C., Norimatsu, Y., Iwasawa, S., Tsuda, T., and Ogawa, H. (2007) *Proc. Natl. Acad. Sci. U.S.A.* **104,** 19831–19836
49. Laursen, M., Bublitz, M., Moncoq, K., Olesen, C., Møller, J. V., Young, H. S., Nissen, P., and Morth, J. P. (2009) *J. Biol. Chem.* **284,** 13513–13518
50. Toyoshima, C., and Mizutani, T. (2004) *Nature* **430,** 529–535
51. Toyoshima, C., Nakasako, M., Nomura, H., and Ogawa, H. (2000) *Nature* **405,** 647–655
52. Champeil, P., Menguy, T., Soulié, S., Juul, B., de Gracia, A. G., Rusconi, F., Falson, P., Denoroy, L., Henao, F., le Maire, M., and Moller, J. V. (1998) *J. Biol. Chem.* **273,** 6619–6631
53. Abu-Abed, M., Mal, T. K., Kainosho, M., MacLennan, D. H., and Ikura, M. (2002) *Biochemistry* **41,** 1156–1164
54. Hilge, M., Siegal, G., Vuister, G. W., Güntert, P., Gloor, S. M., and Abrahams, J. P. (2003) *Nat. Struct. Biol.* **10,** 468–474